International Immunopharmacology 125 (2023) 111132

Contents lists available at ScienceDirect

International Immunopharmacology

journal homepage: www.elsevier.com/locate/intimp

Activation of cGAS-STING signaling pathway promotes liver fibrosis and hepatic sinusoidal microthrombosis

Shaobin Luo [b], Rongkun Luo [b], Huanyuan Lu [b], Rui Zhang [b], Gang Deng [b], Hongwu Luo [b], Xiao Yu [b], Changfa Wang [b], Hui Zhang [b], Yuping Zhang [b], Wei Huang [b], Jichun Sun [b], Yinghong Liu [a], Feizhou Huang [b], Zhao Lei [b,*]

[a] The Third Xiangya Hospital of Central South University, Surgery Center, 138 Tongzipo Road, Changsha City, Hunan Province, China
[b] The Third Xiangya Hospital of Central South University, Department of Hepatopancreatobiliary Surgery, 138 Tongzipo Road, Changsha City, Hunan Province, China

ARTICLE INFO

Keywords:
Liver fibrosis
Hepatic inflammation
RNA-Seq
cGAS-STING signaling pathway
Hepatic sinusoidal microthrombosis
Portal vein pressure gradient
Portal hypertension

ABSTRACT

Inflammation plays an essential role in the development liver fibrosis.The Cyclic guanosine monophosphate-adenosine monophosphate synthase (cGAS) is a central cytoplasmic DNA sensor which can recognize cytoplasmic DNA, known to trigger stimulator of interferon genes (STING) and downstream proinflammatory factors. Here, we investigated the role of cGAS-STING signaling pathway in the pathogenesis of liver fibrosis.Differentially expressed genes (DEGs) in human liver tissue were identified using RNA-Seq analysis. As models of liver fibrosis, chronic Carbon tetrachloride (CCl_4) exposure were applied in cGAS-knockout mice. LX-2 cells were co-cultured with human liver sinusoidal endothelial cells (LSECs) to explore the underlying mechanisms of hepatic sinusoidal microthrombosis in an inflammatory microenvironment. The endoscopic ultrasound-guided portal vein pressure gradient (EUS-PPG) method was used to analyze the associations between hepatic sinusoidal microthrombosis and PPG in patients with liver fibrosis and portal hypertension (PTH). The RNA-seq analysis results showed that DEGs were enriched in inflammation and endothelial cell activation. The upregulation of the cGAS-STING signaling exacerbated liver fibrosis and intrahepatic inflammation. It also exacerbated LSECs impairment and increased the contribution of hepatic sinusoidal microthrombosis to liver fibrosis in vivo and in vitro. Prothrombotic mediators and proinflammatory factors were associated with PPG in patients with liver fibrosis and portal hypertension. Therefore, activating cGAS-STING signaling pathway promotes liver fibrosis and hepatic sinusoidal microthrombosis, which may lead to increased portal vein pressure.

1. Introduction

Liver fibrosis is caused by chronic hepatocyte injury, which can result from viral infection, alcoholic liver disease, or nonalcoholic steatohepatitis [1]. Inflammation is an important and complex feature of liver fibrosis. Following liver injury, inflammatory cells, and the innate immune system lead to liver fibrosis mediated by hepatic stellate cells (HSCs) activation and extracellular matrix (ECM) deposition. HSCs are closely connected to liver sinusoidal endothelial cells (LSECs) in the space of Disse and modulate their activity by sinusoidal communication [2,3]. In the development of liver fibrosis, LSECs are damaged and changed phenotypes that promote hepatic sinusoidal microthrombosis, which leads to the exacerbation of intrahepatic vascular resistance and portal hypertension (PHT) [4–6]. However, to our knowledge, the underlying mechanisms of intrahepatic inflammation in liver fibrosis have not been elucidated.

Continuous efforts have been made to unveil the mysteries behind liver fibrosis using system biology approaches, including genomics and transcriptomics analysis. In our study, RNA sequencing analysis was used to evaluate gene expression in liver fibrosis. Bioinformatics analysis showed that inflammaory pathways were significantly activated during liver fibrosis. The cGAS-STING signaling pathway is a crucial innate immune and inflammatory pathway in mammals. Previous studies reported that the potential impact of the cGAS-STING signaling pathway in liver ischemia–reperfusion injury, nonalcoholic steatohepatitis, hepatic B virus infection, and other liver diseases has recently attracted widespread attention [7]. The inflammatory response can be promoted through the cyclic guanosine monophosphate adenosine synthase

* Corresponding author.
E-mail address: leizhao1987@outlook.com (Z. Lei).

https://doi.org/10.1016/j.intimp.2023.111132
Received 22 June 2023; Received in revised form 15 October 2023; Accepted 23 October 2023
Available online 9 November 2023

(cGAS)–stimulator of interferon genes (STING) pathway [8,9]. cGAS is a cytoplasmic DNA sensor; upon recognition of viral DNA or mitochondrial DNA, it synthesizes 2,3-cyclic guanosine–adenosine monophosphate (2,3-cGAMP), which activates STING [8]. Subsequently, STING forms a complex with TANK-binding kinase 1 (TBK1), which phosphorylates transcription factors such as interferon regulatory factor 3 (IRF3), inducing the synthesis of type I interferon (IFN-β) and inflammatory cytokines [10,11]. There is evidence that the cytosolic DNA content of damaged hepatocytes is significantly increased, and the cGAS-STING signaling pathway is activated to an enhanced inflammatory response in the liver [12–16].

Based on the previous findings, we hypothesized that activation of the cGAS-STING signaling pathway contributes to liver fibrosis by promoting intrahepatic inflammation. Thus, we investigated the role of cGAS-STING signaling pathway in the pathogenesis of liver fibrosis, and our results may provide insights that facilitate the treatment of liver fibrosis.

2. Materials and methods

2.1. Human serum and liver samples

Serum specimens were derived from 40 patients with diagnosed liver fibrosis. Liver fibrosis tissues were from 12 of these patients who experienced liver puncture biopsy. Normal liver tissues (n = 12) from patients with hepatic hemangioma were served as controls. 4 cases of liver fibrosis and normal liver tissues were for RNA-seq, and the rest were used for follow-up studies. Each specimen received a histological score by using the Ishak system [17]. All patients informed possible risks and signed the consent form. The study protocol was approved by the Clinical Ethics Committee of the Third Xiangya Hospital (approval number: I-22217).

2.2. RNA extraction and library construction

Total RNA was isolated and purified using TRIzol reagent (Invitrogen, USA) following the manufacturer's procedure. The RNA amount and purity of each sample was quantified using NanoDrop (Wilmington, USA). The RNA integrity was assessed by Bioanalyzer 2100 (Agilent, USA) with RIN number >7.0, and confirmed by electrophoresis with denaturing agarose gel. Poly (A) RNA is purified from 1 μg total RNA using Dynabeads Oligo (dT)25–61005 (Thermo Fisher, USA) using two rounds of purification. Then the poly(A) RNA was fragmented into small pieces using Magnesium RNA Fragmentation Module (NEB, USA) under 94 °C 5–7 min. Then the cleaved RNA fragments were reverse-transcribed to create the cDNA by SuperScript™ II Reverse Transcriptase (Invitrogen, USA), which were next used to synthesise U-labeled second-stranded DNAs with E. coli DNA polymerase I (NEB, USA), RNase H (NEB, USA) and dUTP Solution (Thermo Fisher, USA). An A-base is then added to the blunt ends of each strand, preparing them for ligation to the indexed adapters. Each adapter contains a T-base overhang for ligating the adapter to the A-tailed fragmented DNA. Single- or dual-index adapters are ligated to the fragments, and size selection was performed with AMPureXP beads. After the heat-labile UDG enzyme (NEB, cat.m0280, USA) treatment of the U-labeled second-stranded DNAs, the ligated products are amplified with PCR by the following conditions: initial denaturation at 95 °C for 3 min; 8 cycles of denaturation at 98 °C for 15 s, annealing at 60 °C for 15 s, and extension at 72 °C for 30 s; and then final extension at 72 °C for 5 min. The average insert size for the final cDNA library was 300 ± 50 bp. At last, we performed the 2 × 150 bp paired-end sequencing (PE150) on an illumina Novaseq™ 6000 (LC-Bio Technology, China) following the vendor's recommended protocol.

2.3. Bioinformatics analysis of RNA-seq

Fastp software (https://github.com/OpenGene/fastp) were used to remove the reads that contained adaptor contamination, low quality bases and undetermined bases with default parameter. Then sequence quality was also verified using fastp. We used HISAT2 to map reads to the reference genome of Homo sapiens GRCh38. The mapped reads of each sample were assembled using StringTie (https://ccb.jhu.edu/software/stringtie) with default parameters. Then, all transcriptomes from all samples were merged to reconstruct a comprehensive transcriptome using gffcompare (https://github.com/gpertea/gffcompare/). After the final transcriptome was generated, StringTie and was used to estimate the expression levels of all transcripts. StringTie was used to perform expression level for mRNAs by calculating FPKM. The differentially expressed mRNAs were selected with fold change > 2 or fold change < 0.5 and with parametric F-test comparing nested linear models (p value < 0.05).

2.4. Animals

To produce liver fibrosis animal models, C57BL/6J mice (Lake Jingda, China) and cGAS-KO mice (Jackson Lab, No: 026554, USA) of 6-week-old were injected intraperitoneally twice a week for eight weeks with either olive oil alone (5 ml/kg) or carbon tetrachloride (CCl_4) (1:4 in olive oil) (RHAWN, China). Construction of STING overexpression mice as follows: C57BL/6J mice were intramuscular injected with 2,3-cGAMP (500 μg/kg, InvivoGen, USA) three times a week for 2 weeks. Afterwards, the mice were anaesthetized using chloral hydrate before being killed. Their serum and liver tissues were collected and stored at −80 °C. The experimental animal protocol was approved by the Institutional and Local Committee on the Care and Use of Animals of the Central South University (approval number: CSU-2022–0428).

2.5. Liver histology

Liver samples from mice and humans were embedded in paraffin after being fixed in 4 % paraformaldehyde. Sections (4 μm) were prepared, then stained with hematoxylin-eosin (HE) and Masson's trichrome. Collagen deposition was analyzed using Masson's trichrome staining. Ndp.view software (Hamamatsu, Japan) was used to evaluate hepatic sinusoidal microthrombosis in digitally scanned pathological sections. Random observation 100 hepatic sinusoidal vessels, and the thrombosis rate was calculated. Representative images of sections are shown in this article.

2.6. Measurement of portal pressure gradient

Each patient was placed in the left supine position and administered intravenous anesthesia. The liver was scanned by endoscopic ultrasound (EUS) (EG-3870UTK, PENTAX, Japan); the first and second hepatic portal were exposed; and the main portal vein and left hepatic vein were both located [18]. The portal vein near the intrahepatic bifurcation was entered through the stomach, whereas the hepatic vein or retrohepatic inferior vena cava was entered through the stomach [18]. Select the hepatic vein that is almost parallel to the probe and use a 25G puncture needle connected to a pressure sensor to perform puncture and pressure measurement through the stomach and the liver or through the duodenum and the liver. Likewise, intrahepatic branches of the portal vein were confirmed by endoscopic ultrasonography to identify the appearance of hyperechoic walls and unidirectional blood flow using color Doppler ultrasound. After a successful puncture, 1 ml of heparin saline should be injected. If water bubbles appear in the blood vessel under Doppler ultrasound, it means that the puncture needle has entered the lumen of the target blood vessel. The EUS-guided portal vein pressure gradient (EUS-PPG) measurement procedure is summarized in Supplementary Fig. 1. After the pressure had been stabilized for 30–60 s,

readings were recorded. Each measurement was repeated three times, and the PPG was calculated using the mean of the three readings. All patients informed possible risks and signed the consent form. The study protocol was approved by the Clinical Ethics Committee of the Third Xiangya Hospital (approval number: I-22217).

2.7. Reverse transcription quantitative polymerase chain reaction (RT-qPCR)

Total RNA was extracted from lysates of liver tissue and cells using TRIzol (Thermo, China). Equal amounts of total RNA (1 μg) was then used as the template for reverse transcription of cDNA. SYBR Green reagent (Abiowell, China) was used for RT-qPCR. The RT-qPCR protocol consisted of 10 min at 95 °C and 40 cycles at 60 °C for 15 s each. Primer sequences are listed in Supplementary Table 2.

2.8. Western blotting (WB)

RIPA lysis buffer (Abiowell) was used to extract whole protein from cells or liver tissues. The protein was transferred to a nitrocellulose filter membrane. Each membrane was incubated with primary antibody for 12 h at 4 °C, then washed three times with horseradish peroxidase-conjugated secondary antibody (1:5000 dilution, Abiowell). Analysis Software (Bio-Rad Laboratories, USA) was used for densitometric measurement of each band. The primary antibodies were as follows: cGAS (1:1000, CST, USA), STING (1:1000, Abcam, USA), Phospho-STING (1:1000, Abcam, USA), Col-1α1 (1:1000, Proteintech, USA), β-actin (1:5000, Proteintech, USA) and GAPDH (1:5000, Proteintech, USA).

2.9. Transmission electron microscopy (TEM) analyses

Liver specimens and cell samples were fixed with 2.5 % glutaraldehyde for 12 h. Then, the samples were immersed in propylene oxide and soaked for 3 h in epoxy resin. Ultrathin sections (80 nm) were stained with uranyl acetate and lead citrate. A transmission electron microscope (JEOL, Japan) was used to visualize each section.

2.10. Cell culture and transfection

LX-2 cells (Procell Life Science&Technology, China) were cultured in DMEM supplemented with 10 % fetal bovine serum, 1 mmol/L L-glutamine, and 100 IU/ml penicillin. After 24 h of pretreatment with transforming growth factor (TGF)-β1 (20 ng/mL; PeproTech, China), the cells were collected for use in experiments. Prior to transfection, LX-2 cells were cultivated in six-well plates until they reached approximately 70 % confluence. Lipofectamine 2000 transfection reagent (Invitrogen, China) was used for transfection of cGAS- and STING-overexpressing plasmids, as well as small interfering RNAs (siRNAs) targeting cGAS and STING (TransSheep Bio, China).

2.11. Cell viability analysis

The viability of LX-2 cells was measured using the cell counting kit (CCK)-8 assay. LX-2 cells were plated in 96-well plates (5×10^3 cells/well), then exposed to various concentrations of TGF-β1 for 24 h. Subsequently, the cells were incubated with CCK-8 for 2 h at 37 °C. A microplate reader was used to measure absorbance at 450 nm (Huisong Tech, China).

2.12. Co-culture of LX-2 cells and LSECs

LX-2 cells were transfected with cGAS and STING overexpressing plasmids and siRNA. Cells were collected from each group, then treated for 24 h with TGF-β1 (20 ng/mL). Human LSECs (iCell Bioscience, China) were cultured overnight in the special culture medium serum (iCell Bioscience, China). Subsequently, LX-2 cells and LSECs were washed with phosphate-buffered saline, then detached from their respective culture flasks via trypsinization. Next, LX-2 cells were seeded in the upper chambers of a Transwell co-culture plate (1×10^5 cells/well), whereas LSECs were seeded in the lower chambers of a Transwell co-culture plate (1×10^5 cells/well).

2.13. Statistical analysis

GraphPad Prism 8 software was used for statistical analysis. Data are shown as means ± SEM. Statistical differences were analyzed by unpaired Student's t-tests between two groups and one-way ANOVA with the Bonferroni correction among multiple groups. Correlation was examined by linear regression. P-values < 0.05 were considered statistically significant.

3. Results

3.1. RNA-Seq and differentially expressed gene analysis

To evaluate the differential expression patterns of genes associated with liver fibrosis, total RNA was extracted from the liver tissues of patients with liver fibrosis and control group. A total of 451 genes (1.20 % of the total 37415 genes) were reported as significant DEGs, which comprised 186 upregulated genes (accounting for 41.24 % of all significant DEGs) and 265 downregulated genes (accounting for 58.76 % of all significant DEGs), respectively (Fig. 1A). The gene expression of inflammatory factors and endothelial factor was increased in liver fibrosis (Fig. 1B and C). The bubble map of KEGG enrichment analysis indicated significant changes in cytokine - cytokine receptor interaction, cell cycle signaling pathway, cell adhesion signaling pathway, chemokine signaling pathway, toll-like receptor signaling pathway (Fig. 1D). Further GSEA analysis showed that the enrichment score of cGAS-STING signaling pathway in the hepatic fibrosis group changed significantly compared with that in the control group (Fig. 1E), suggesting that the cGAS-STING signaling pathway plays an important role in liver fibrosis. Protein interaction network diagram of genes showed the interaction between inflammatory factors and endothelial factor was powerful. The expression of inflammatory factors NF-κB, IL-1β, and IL-6 was high, mostly held by STING and TBK1(Fig. 1 F). Further, the upstream signaling pathway of endothelial activation was regulated primarily by vWF, Angpt-2 and KLF2.

3.2. cGAS-STING signaling pathway is activated in liver fibrosis

Compared with healthy human liver specimens, fibrotic liver specimens exhibited higher Ishak score in HE staining; moreover, Masson's trichrome staining revealed a greater percentage of collagen-positive area in fibrotic liver specimens (Fig. 2A). Obviously, fibrotic marker α-SMA significantly increased in fibrotic liver specimens (Fig. 2B). WB and RT-qPCR displayed that the expression of cGAS, STING, TBK1, and IRF3 were higher in fibrotic liver specimens than in healthy liver specimens (Fig. 2C and D). Additionally, fibrotic liver specimens exhibited an enhanced inflammatory response, as indicated by the levels of inflammatory factors (IL-1β, IL-6, CXCL-1, and IFN-β) (Fig. 2E).

Next, CCl_4-induced liver fibrosis mouse model was established to explore the role of the cGAS-STING signaling pathway in liver fibrosis. HE and Masson's trichrome staining results suggested that hepatic fibrogenesis was increased in CCl_4-treated mice, compared with wild-type (WT) mice (Fig. 2F). Similarly, quantitative analysis of staining results showed that, with increasing modeling time, mice had a higher Ishak score and greater percentage of collagen-positive areas (Fig. 2G and H). Furthermore, the level of α-SMA expression gradually increased after 4, 6 and 8 weeks of modeling, compared with WT mice (Fig. 2I). WB and RT-qPCR analysis of liver specimens showed strong upregulation of cGAS and STING expression levels in mice with increasing modeling time (Fig. 2J and K). RT-qPCR revealed that the expression

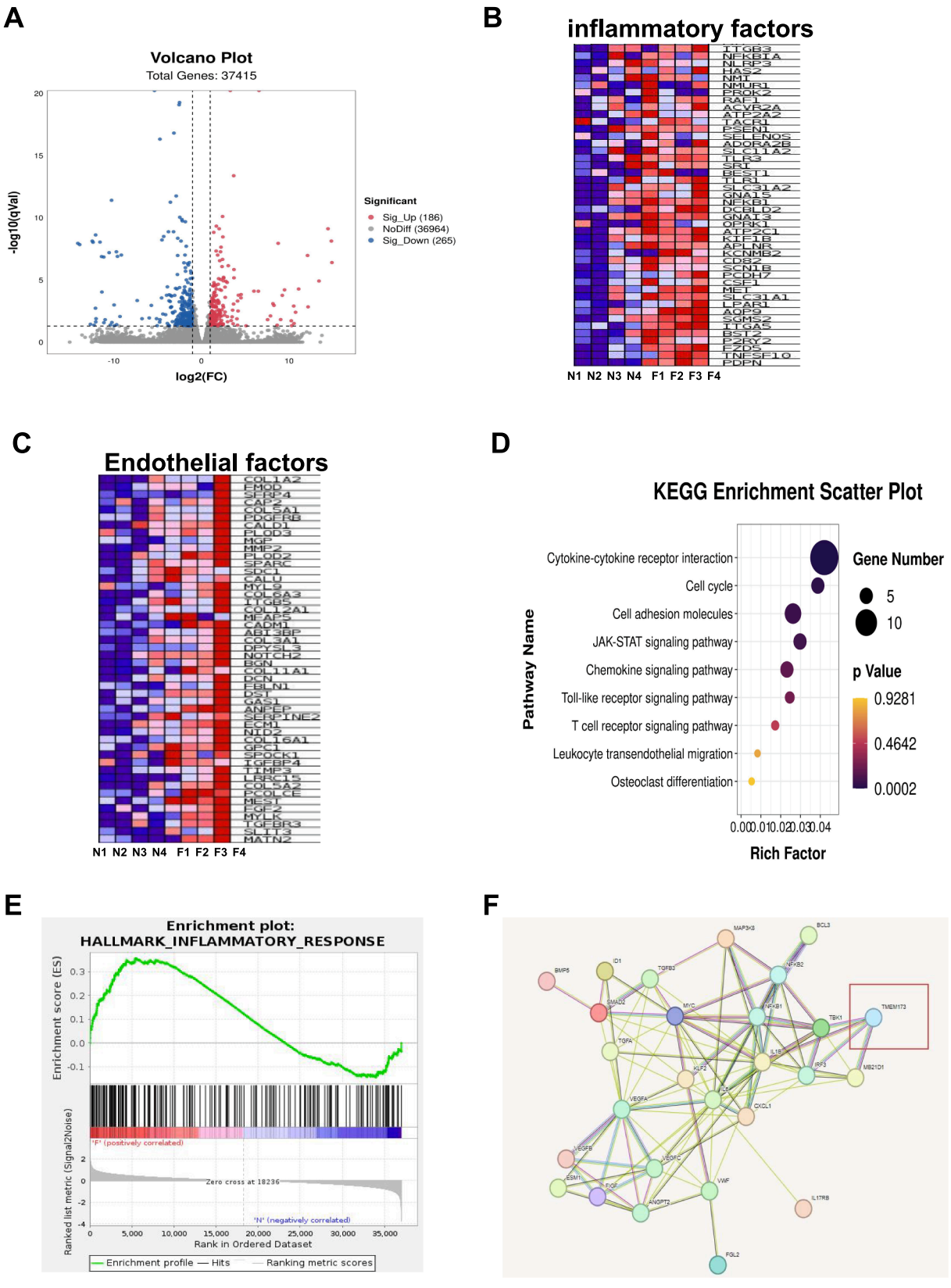

Fig. 1. RNA-seq bioinformatics analysis. Differential gene volcano map in liver fibrosis (A). Inflammatory factors expression heat map in liver fibrosis (B). Endothelial factors expression heat map in liver fibrosis (C). KEGG enrichment analysis of bubbles (D). GSEA pathway enrichment score (E). Protein interaction network diagram of genes in liver fibrosis (F).

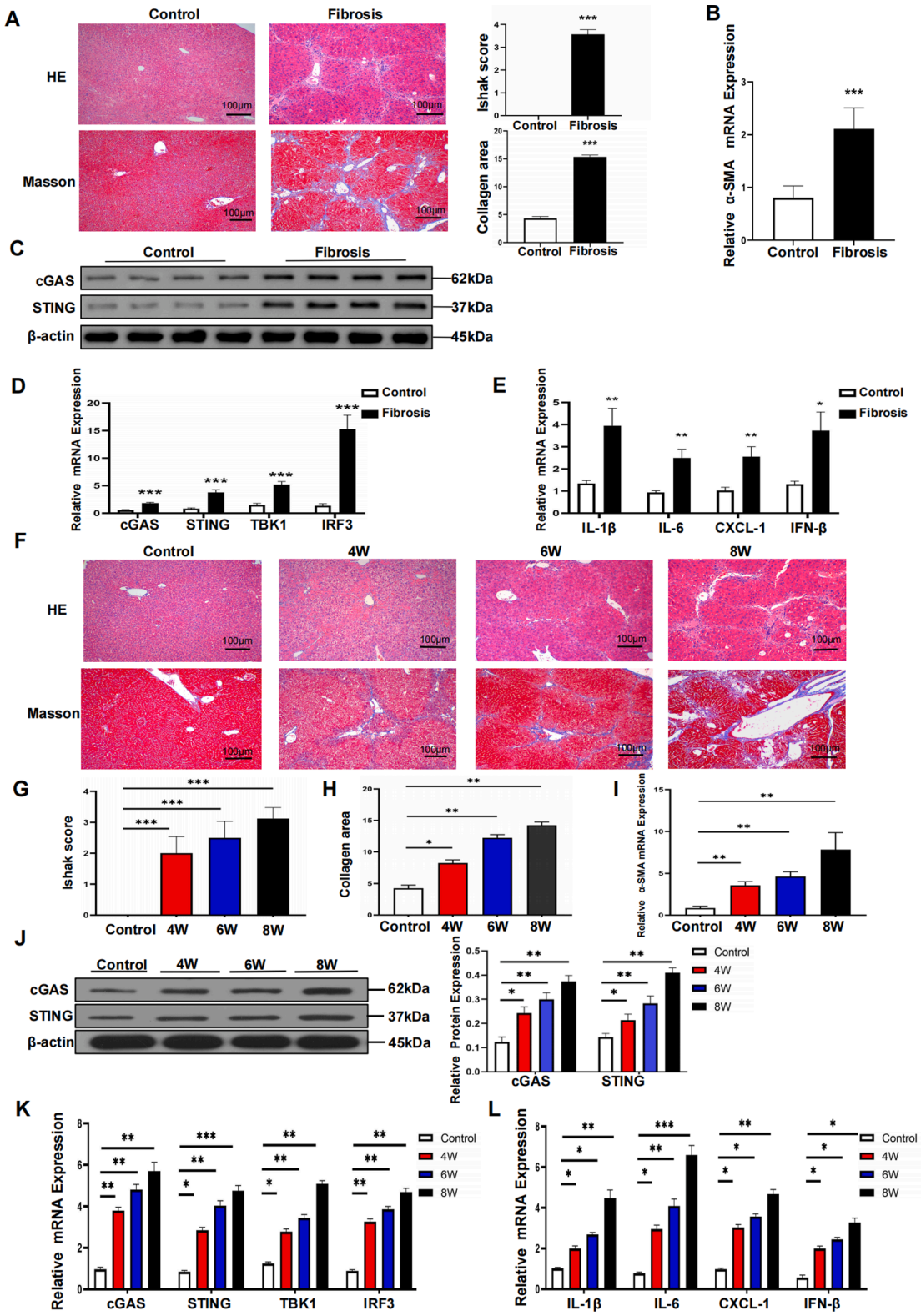

Fig. 2. cGAS-STING signaling pathway is activated in liver specimens from patients and mice with liver fibrosis. Sections of liver specimens from healthy volunteers (n = 8) and patients with fibrosis (n = 8) were analyzed by HE and Masson's trichrome staining (original magnification 100); areas of positive staining were measured by ImageJ software (A). Levels of α-SMA mRNA expression in healthy volunteers and patients with fibrosis (B). Protein and mRNA expression levels of cGAS-STING signaling pathway components (C and D). Relative mRNA expression levels of IL-1β, IL-6, CXCL-1, and IFN-β in patients with liver fibrosis (E). WT mice were injected with CCl_4 or vehicle for 8 weeks. HE and Masson's trichrome staining of liver specimens with modeling times of 4, 6, and 8 weeks (original magnification × 100) (F). Quantitative analysis of HE staining and areas of positive collagen staining (G and H). mRNA levels of α-SMA expression in fibrosis model mice with increasing modeling time (I). Analysis of the cGAS and STING by WB and RT-qPCR in liver specimens with different modeling times (J and K). Expression levels of inflammatory factors, including IL-1β, IL-6, CXCL-1, and IFN-β, gradually elevated in liver specimens with increasing modeling time (L). Data are shown as means ± standard errors of the mean. *: $P < 0.05$; **: $P < 0.01$; ***: $P < 0.001$ vs. control group.

levels of inflammatory factors including IL-1β, IL-6, CXCL-1, and IFN-β in fibrotic liver specimens were considerably upregulated with increasing modeling time (Fig. 2L). In summary, these results showed that the cGAS-STING signaling pathway is activated in patients and mice with liver fibrosis. Furthermore, inflammatory factors are produced in fibrotic liver tissue.

3.3. cGAS-STING signaling pathway exacerbates CCl_4-induced liver fibrosis in mice

To explore the role of the cGAS-STING signaling pathway during the progression of liver fibrosis, we used CCl_4 to induce liver fibrosis for 8 weeks in cGAS-KO mice and STING-activated mice. Compared with model mice lacking the cGAS-KO modification, inhibition of the cGAS-STING signaling pathway markedly attenuated liver fibrosis, leading to a decreased Ishak score and smaller percentage of collagen-positive areas (Fig. 3A–C). Additionally, the expression of α-SMA was considerably lower in liver specimens from cGAS-KO mice (Fig. 3D). Western blot revealed that cGAS gene expression was completely abolished (Fig. 3E). The mRNA levels of cGAS-STING signaling pathway mediators and inflammatory indicators in cGAS-KO mice were substantially reduced (Fig. 3F and G).

Next, we used 2,3-cGAMP to activate the expression of STING in WT mice. Upon exposure to CCl_4, cGAMP-induced STING activation strongly promoted liver fibrosis, characterized by an increased Ishak score and larger percentage of collagen-positive areas (Fig. 3H–J). Furthermore, the expression of α-SMA was higher in liver specimens from STING-activated mice (Fig. 3K). After 8 weeks of fibrosis induction, STING-activated mice exhibited strongly positive expression of the cGAS-STING signaling pathway and inflammatory factors, compared with fibrotic mice established for 8 weeks (Fig. 3L–N). These findings confirmed that upregulation of the cGAS-STING signaling pathway could exacerbate liver fibrosis in vivo.

3.4. Inhibition of cGAS-STING signaling pathway alleviates TGF-β1-induced profibrotic gene expression in HSCs

Next, the role of cGAS-STING signaling pathway in liver fibrosis was investigated in vitro. LX-2 cells, a human HSC line, were transfected with cGAS-siRNA and STING-siRNA respectively. The protein expression of cGAS and STING were significantly reduced in the corresponding siRNA groups, compared with the si-NC-treated group (Fig. 4A–D). LX-2 cells were treated with various concentrations of TGF-β1 for 24 h to induce HSC activation. After treatment with TGF-β1, the expression of α-SMA in LX-2 cells was elevated in a dose-dependent manner. CCK-8 assay and RT-qPCR showed that 20 ng/mL TGF-β1 had the greatest effect on activation of LX-2 cells (Fig. 4E and F). Thus, 20 ng/mL TGF-β1 was used in subsequent experiments. Additionally, cGAS-siRNA-transfected and STING-siRNA-transfected LX-2 cells were treated with TGF-β1 for 24 h. Compared with TGF-β1-activated LX-2 cells, the Col-1α1 protein levels and α-SMA mRNA levels were decreased after knocking down cGAS or STING (Fig. 4G and H). Moreover, cGAS-STING signaling pathway activation and inflammatory cytokine expression were substantially reduced in the cGAS-siRNA and STING-siRNA group (Fig. 4I and J). Overall, the results indicated that inhibition of the cGAS-STING signaling pathway in HSCs significantly attenuated the expression of profibrotic genes and inflammatory cytokines.

3.5. Activition of cGAS-STING signaling pathway aggravates profibrotic gene and inflammatory cytokine expression in HSCs

Subsequently, plasmid of cGAS-OE and STING-OE were transfected into LX-2 cells to overexpress cGAS and STING, respectively. Compared with the negative control, there was a noteworthy increase in the cGAS and STING expression in the transfected LX-2 cells measured by WB (Fig. 5A–D). LX-2 cells were transfected with cGAS-OE and STING-OE to overexpress cGAS and STING, then treated with TGF-β1 for 24 h. The Col-1α1 protein levels and α-SMA mRNA levels were increased compared with TGF-β1-activated LX-2 cells (Fig. 5E and F). Then the crucial gene of cGAS-STING pathway and inflammatory cytokine in overexpressed plasmid group were remarkably elevated (Fig. 5G–J). These findings show that the up-regulation of cGAS-STING signaling pathway in HSCs aggravates inflammatory response and forms an inflammatory microenvironment in the liver.

3.6. Activation of cGAS-STING signaling pathway in HSCs exacerbates LSEC impairment

To explore the mechanism by which the intrahepatic inflammatory microenvironment caused by the activation of cGAS-STING signaling pathway in HSCs contributes to LSEC impairment, we performed a co-culture experiment involving LX-2 cells and LSECs (Fig. 6A). LX-2 cells were transfected with cGAS-OE, STING-OE, cGAS-siRNA, or STING-siRNA; they were then treated with 20 ng/mL TGF-β1 for 24 h. Collected LSECs of groups including control group, TGF-β1 group, si-cGAS group, cGAS-OE group, si-STING group, and STING-OE group. Cell morphology and microstructural changes were observed by TEM. Normal LSECs were flat, with intact organelles (Fig. 6B). In the TGF-β1 group, LSECs exhibited nearly round nuclei, with some damaged mitochondria and some pseudopodia (Fig. 6C). In the si-cGAS and si-STING groups, LSECs exhibited substantially less damage, with significantly fewer damaged mitochondria and pseudopodia (Fig. 6D and F). In the cGAS-OE and STING-OE groups, LSECs lost their normal morphology, organelles were destroyed, and the numbers of pseudopodia were markedly increased (Fig. 6E and G). Further, we quantified the number of LSECs pseudopods in each group which is closely related to morphological changes of LSECs when they are under different degrees of external stimulation and injury (Fig. 6H).These data demonstrate that the activation of cGAS-STING signaling pathway in HSCs exacerbates LSEC impairment in a co-culture system. KLF2, an early indicator of LSEC damage, was significantly increased expression in LSECs during co-culture with up-regulated cGAS and STING gene (Fig. 6I). Furthermore, we observed that injured LSECs released vasoactive substances including angiopoietin-2 (Angpt-2) and thrombomodulin (TM) (Fig. 6J and K), which can disrupt coagulatory homeostasis in the microcirculation and promote the onset of thrombosis. Angpt-2, a glycoprotein secreted by endothelial cells, can stabilize newly formed thrombosis [19]. TM, a thrombin regulatory protein on the surface of endothelial cells, exhibits an anticoagulatory function [20]. Therefore, we speculated that LSECs were damaged during the progression of liver fibrosis, then participated in further development of liver fibrosis via secretion of vasoactive substances.

3.7. cGAS-STING signaling pathway exacerbates damage to LSECs in mice with liver fibrosis

To examine the detrimental effect of activated HSCs on LSECs in vivo, TEM analysis was employed in liver tissues of WT, 4 and 8 weeks of modeling mice, cGAS-KO and STING-actived model mice. No abnormalities in liver cell ultrastructure were observed in the control group (Fig. 7A; red arrows indicate LSECs). After 4 weeks of liver fibrosis modeling, the hepatic sinusoidal vascular lumen was ruptured, the hepatic microvilli were reduced, and few collagen fiber bundles were present in perisinusoidal space. The presence of discontinuous basement membrane (red arrow) in the subendothelium suggested that hepatic sinusoids had transformed into capillaries (Fig. 7B). CCl_4 exposure led to the exacerbation of liver fibrosis and onset of sinusoidal endothelial cell injury. After 8 weeks of modeling, LSECs were enlarged and exhibited an irregular shape, with reduced cytoplasm volume. The perisinusoidal space was enlarged, and pores were present between endothelial cells. Hepatic sinusoidal obstruction is common during the progression of liver fibrosis. The obstruction mainly involves red blood cells and cell

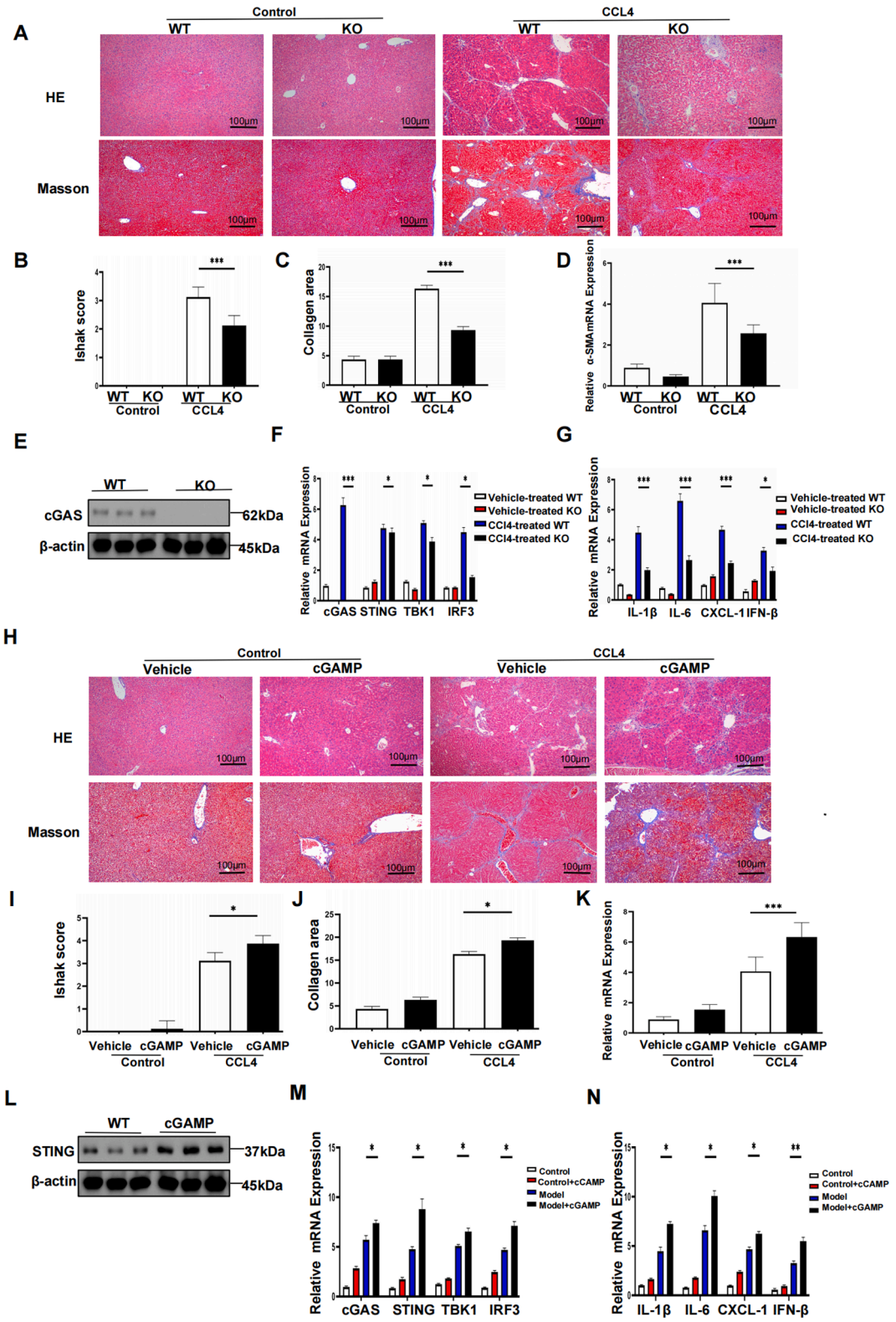

Fig. 3. cGAS-STING **signaling pathway exacerbates CCl_4-induced liver fibrosis in mice.** Wild-type and cGAS-KO mice were administered CCl_4 twice weekly for 8 weeks. Representative images of HE and Masson's trichrome staining results; areas of positive staining were measured by ImageJ software (A–C). Expression levels of α-SMA in WT and cGAS-KO mice administered CCl_4 for 8 weeks (D). Expression levels of cGAS-STING signaling pathway components were analyzed by WB and RT-qPCR (E and F). mRNA expression levels of IL-1β, IL-6, CXCL-1, and IFN-β were analyzed by RT-qPCR (G). Model mice were injected with 2,3-cGAMP twice weekly for 2 weeks. Representative images of HE and Masson's trichrome staining results; areas of positive staining were measured by ImageJ software (H–J). Levels of α-SMA mRNA expression in fibrosis model mice and STING-activated mice administered CCl_4 for 8 weeks (K). Activation of the cGAS-STING signaling pathway was analyzed by WB and RT-qPCR (L and M). The expression levels of IL-1β, IL-6, CXCL-1 and IFN-β were analyzed by RT-qPCR (N). *: $P < 0.05$; **: $P < 0.01$; ***: $P < 0.001$ vs. WT mice administered CCl_4.

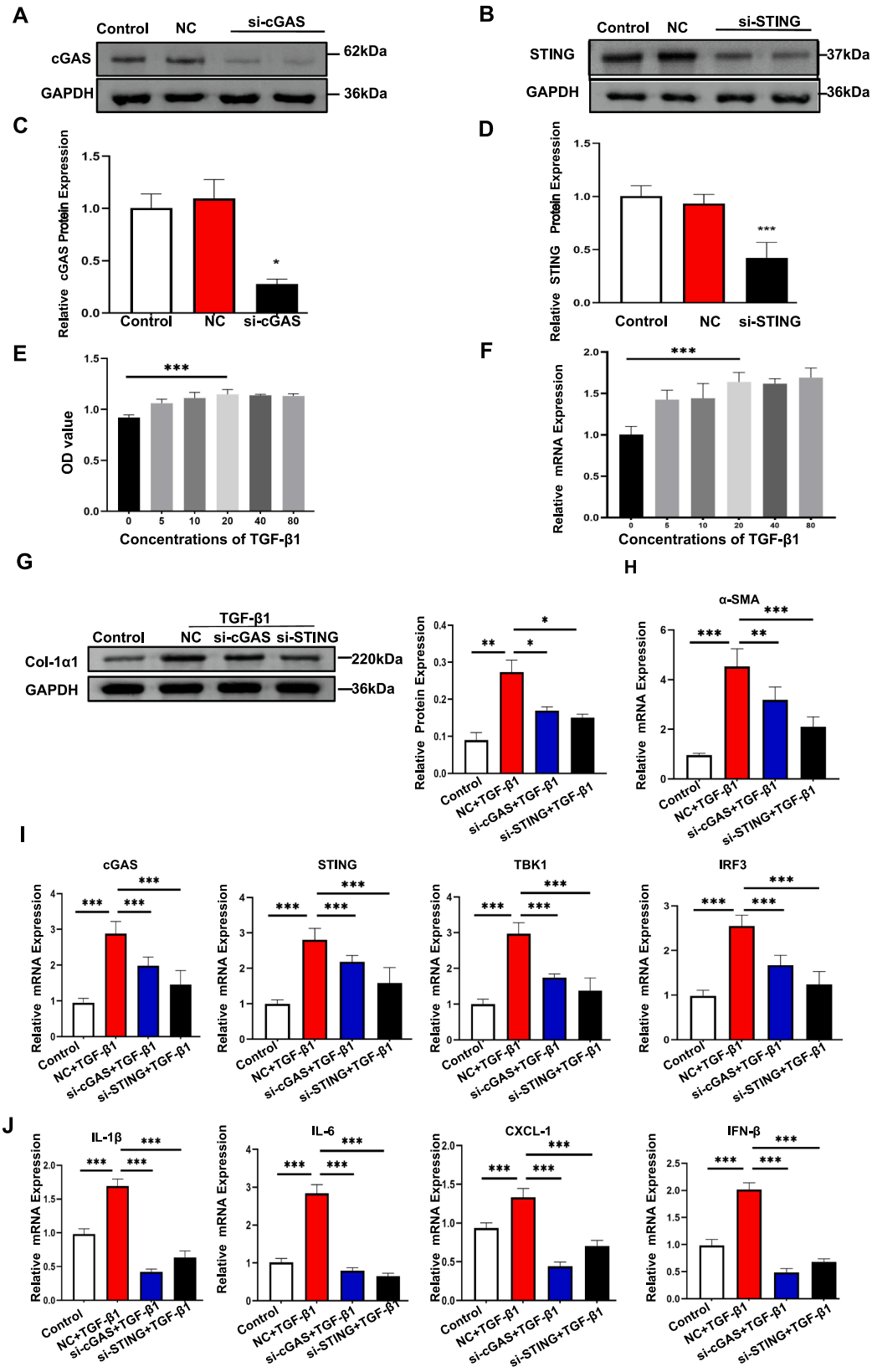

Fig. 4. Inhibition of cGAS-STING signaling pathway alleviates TGF-β1-induced profibrotic gene expression in HSCs. Expression levels of cGAS and STING were measured using WB after transfection with si-NC, cGAS-siRNA or STING-siRNA in LX-2 cells (A–D). LX-2 cells were subjected to CCK-8 assays after treatment with various concentrations of TGF-β1 for 24 h (E). LX-2 cells were transfected with cGAS-siRNA and STING-siRNA, then treated with TGF-β1 (20 ng/mL) for 24 h. The levels of α-SMA mRNA expression and Col-1α1 protein expression were detected (F and G). mRNA expression levels of cGAS, STING, IRF3, TBK1, and inflammatory factors (e.g., IL-1β, IL-6, CXCL-1, and IFN-β) were measured in the control group (untreated LX-2 cells), the model group (activated LX-2 cells), the si-cGAS group, and the si-STING group (I and J). *: $P < 0.05$; **: $P < 0.01$; ***: $P < 0.001$ vs. control group.

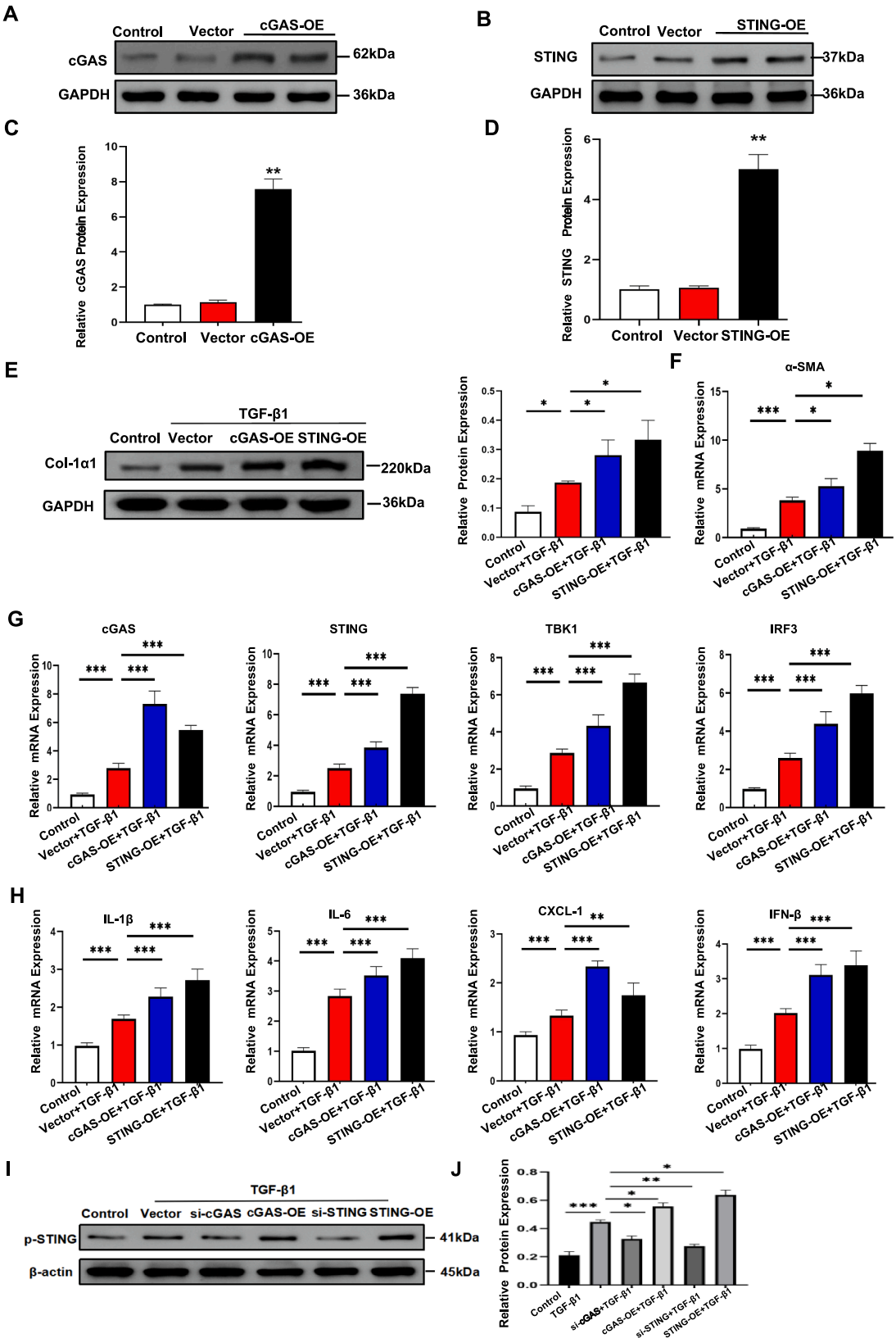

Fig. 5. Overexpression of cGAS-STING signaling pathway exacerbates TGF-β1-mediated activation of HSCs. Expression levels of cGAS and STING were detected by WB after transfection with empty-vector , cGAS-overexpression plasmid or STING-overexpression plasmid (A-D). Transfected LX-2 cells were treated with TGF-β1 (20 ng/mL) for 24 h, then subjected to analysis of Col-1α1 and α-SMA expression levels via RT-qPCR and WB (E and F). mRNA expression levels of cGAS, STING, IRF3, TBK1, and inflammatory factors (IL-1β, IL-6, CXCL-1, and IFN-β) in the control group (untreated LX-2 cells), the model group (activated LX-2 cells), the si-cGAS and si-STING group, the cGAS-OE and STING-OE group (G and H). LX-2 cells were transfected with si-cGAS, si-STING, cGAS-OE or STING-OE, and then treated with TGF-β1. The protein expression of Phospho-STING was determined by Western blotting (I and J). *: $P < 0.05$; **: $P < 0.01$; ***: $P < 0.001$ vs. control group.

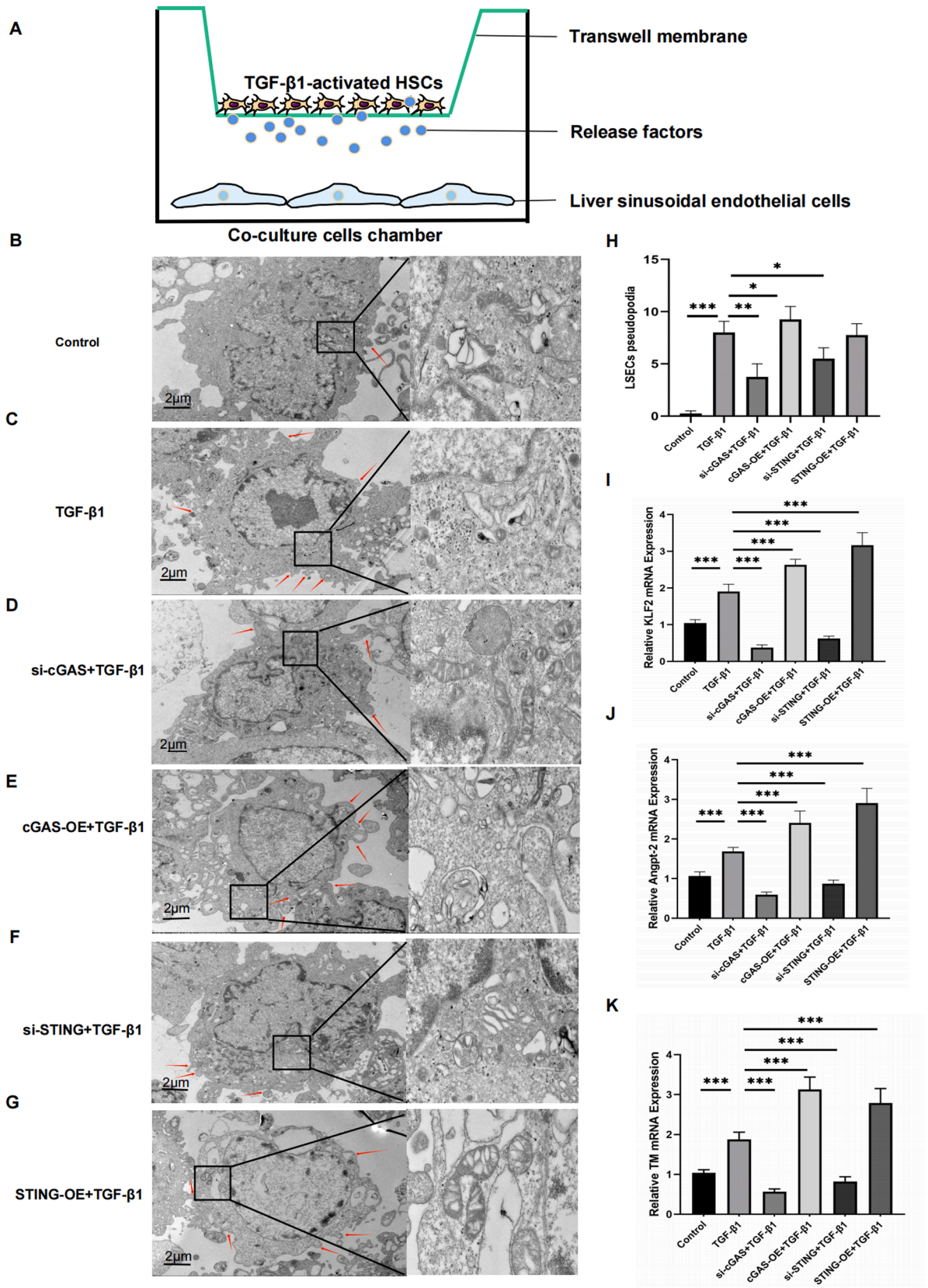

Fig. 6. cGAS-STING **signaling pathway exacerbates the impairment of liver sinusoidal endothelial cells in vitro.** Pretreated LX-2 cells were co-cultured with LSECs for 48 h (A). Collect LSECs in each group in the supernatant of pretreated LX-2 cells. LSEC morphology and microstructural changes were observed and quantified by transmission electron microscopy (B-H). The expression levels of KLF2, Angpt-2, and TM in LSECs were measured by RT-qPCR (I–K). Red arrow indicates pseudopod. *: $P < 0.05$; **: $P < 0.01$; ***: $P < 0.001$ vs. control group.

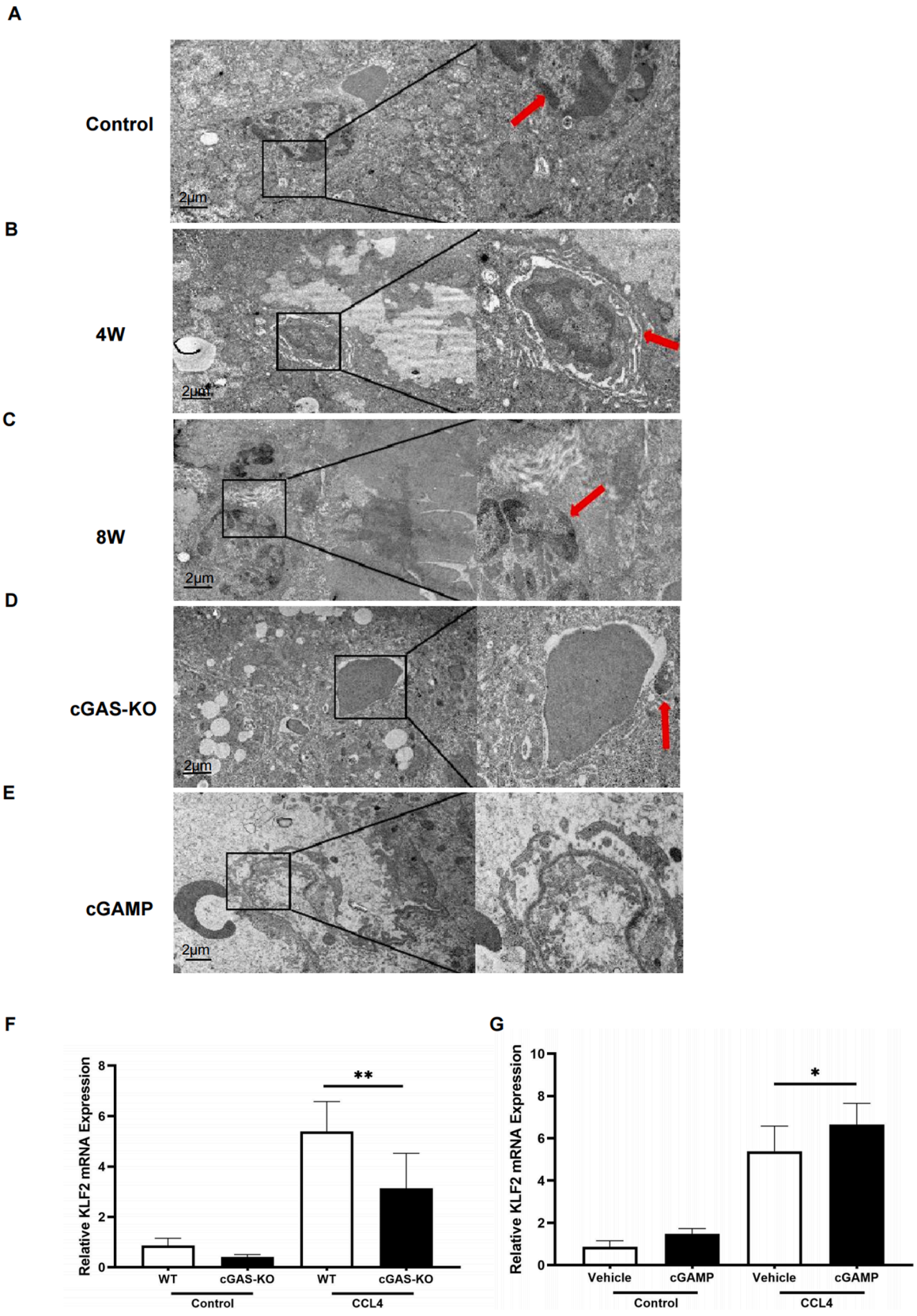

Fig. 7. cGAS-STING **signaling pathway exacerbates damage to liver sinusoidal endothelial cells in vivo.** TEM was used for analysis of liver specimens from WT, 4 and 8 weeks of modeling mice, cGAS-KO and STING-activated mice administered CCl_4 for 8 weeks (A-E). mRNA expression levels of KLF2 in cGAS-KO and STING-activated mice were measured via RT-qPCR (F and G). *: $P < 0.05$; **: $P < 0.01$; ***: $P < 0.001$ vs. WT mice administered CCl_4.

debris, which contribute to the formation of microthrombosis (Fig. 7C). cGAS-KO model mice exhibited less damage to LSECs and their mitochondria (Fig. 7D). In contrast, STING-activated mice had incomplete hepatic sinusoids and disrupted endothelial cell morphology, along with many broken organelles in the perisinusoidal space (Fig. 7E). Notably, STING-actived model mice exhibited greater expression of KLF2 (Fig. 7G), whereas the expression of KLF2 was downregulated in cGAS-KO model mice (Fig. 7F).

3.8. Hepatic sinusoidal microthrombosis is markedly increased in the progression of liver fibrosis

In fibrotic human liver specimens, Masson's trichrome staining revealed prominent hepatic sinusoidal microthrombosis, which differed from the findings in normal human liver specimens (Fig. 8A). The expression levels of the thrombus-forming agents Angpt-2, TM, and von Willebrand factor (vWF) were significantly greater in fibrotic liver

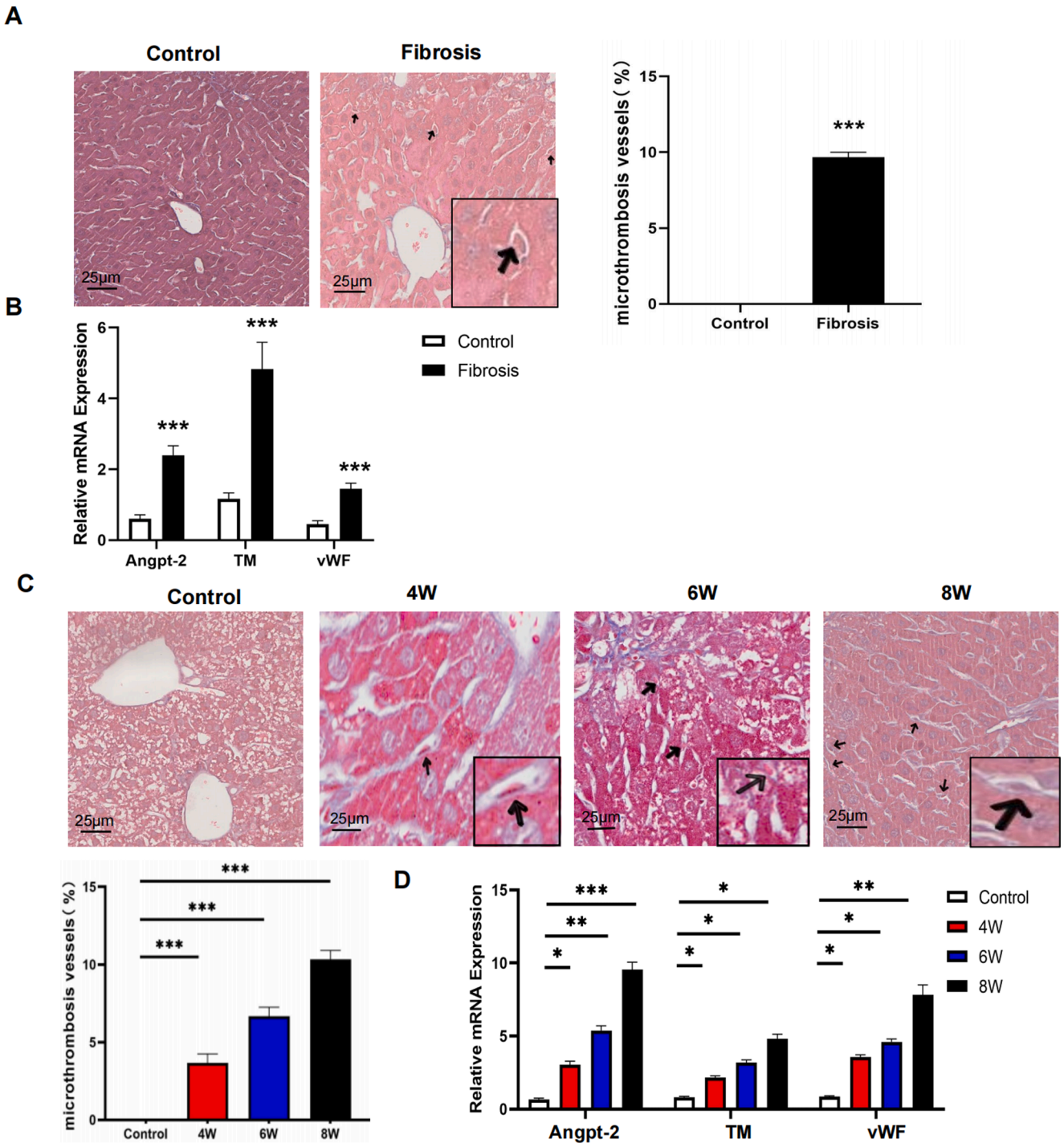

Fig. 8. Hepatic sinusoidal microthrombosis is significantly increased during the progression of liver fibrosis. Masson staining was used to evaluate hepatic sinusoidal microthrombosis in liver specimens from control and patients with fibrosis; the rate of positive vessel staining was measured (A). mRNA expression levels of prothrombotic mediators (Angpt-2, vWF, and TM) were measured (B). Results of Masson staining in mice with modeling times of 4, 6, and 8 weeks; the rate of positive vessel staining was measured (C). mRNA expression levels of Angpt-2, vWF, and TM in mice were measured via RT-qPCR (D). *: $P < 0.05$, **: $P < 0.01$, ***: $P < 0.001$ vs. WT mice administered CCl_4.

specimens than in healthy liver specimens (Fig. 8B). vWF is an important marker for vascular endothelial injury and platelet activation[21]; it promotes platelet activation and aggregation, which have key roles in thrombosis[22]. Similar phenomena were observed in CCl_4-treated mouse liver specimens, in a manner proportional to administration time (Fig. 8C). After CCl_4 treatment, the mRNA levels of Angpt-2, TM, and vWF were gradually increased in mouse liver specimens (Fig. 8D).

3.9. cGAS-STING signaling pathway promotes the formation of hepatic sinusoidal microthrombosis in fibrotic liver

Further exploration of cGAS-STING signaling pathway in hepatic sinusoidal microthrombosis revealed that specimens from cGAS-KO mice showed less hepatic sinusoidal microthrombosis, compared with specimens from WT mice (Fig. 9A). As expected, cGAS-KO mice exhibited lower expression levels of Angpt-2, TM, and vWF (Fig. 9B). In contrast, STING-activated mice showed an increase in the formation of hepatic sinusoidal microthrombosis (Fig. 9C). Additionally, increased expression of Angpt-2, TM, and vWF in STING-activated mice indicate a marked release of prothrombotic substances (Fig. 9D). Thus, we confirmed the involvement of cGAS-STING signaling pathway in the pathogenesis of hepatic sinusoidal microthrombosis in liver fibrosis.

3.10. Prothrombotic mediators are associated with EUS-PPG in patients with liver fibrosis

EUS-PPG was used to evaluate portal vein pressure in patients with liver cirrhosis and PHT. All 40 patients included in this study successfully completed EUS-PPG, and no adverse events occurred in all patients, including gastrointestinal bleeding, gastrointestinal perforation and fistula. The PPG of 40 patients with liver cirrhosis and portal hypertension are shown in the Supplementary Table 1. The serum mRNA level of TM and vWF, as prothrombotic mediators for microthrombosis, had an obvious linear relationship with PPG (Fig. 10A and B). The correlation between the level of Angpt-2 and PPG is not significant (Fig. 10C). These results suggested that hepatic sinusoidal microthrombosis may be an important factor in PHT. The serum mRNA level of IL-1β and IL-6, as proinflammatory factors, have an obvious linear relationship with PPG (Fig. 10D and E). The correlation between the level of CXCL-1 and PPG is insignificant (Fig. 9F). We speculated that inflammatory response might be involved in the formation of portal hypertension.

4. Discussion

Liver fibrosis is a chronic inflammatory process resulting from the recruitment and migration of inflammatory cells and HSCs [23,24]. Our current study demonstrated that the cGAS-STING signaling pathway is activated and exacerbates hepatic inflammation in patients and mice model with liver fibrosis. We analyzed that cGAS was activated as a cytoplasmic DNA sensor in liver fibrosis tissue which may be due to DNA released after mitochondrial damage or hepatitis virus DNA [25]. Activation of cGAS-STING signaling pathway induces IRF3 and NF-kB signaling, leading to the production of inflammatory cytokines and the onset of intrahepatic inflammation [26]. Further, we observed that blockade of the cGAS-STING signaling pathway could attenuate HSCs activation and thus alleviate hepatic fibrosis. Inflammatory factors could activate HSCs and stimulate the synthesis of ECM [27]. During liver injury, inflammatory cells are recruited in the injured site through chemokines attraction [28]. Furthermore, HSCs conversion from a quiescent to an activated state characterized by a myofibroblast-like phenotype responsible for proliferation and excessive extracellular matrix deposition is regulated by inflammatory mediators [29]. These data collectively demonstrated that activation of the cGAS-STING signaling pathway aggravated hepatic inflammation and liver fibrosis.

LSECs are highly specialized endothelial cells representing the interface between blood cells and hepatocytes, and HSCs. In pathological conditions, LSECs play a key role in the initiation and progression of liver fibrosis [30]. Studies have indicated that activation of HSCs affects LSECs and liver homeostasis by secreting vasoactive substance [31,32]. Notably, a major innovation of our research is the co-culture of HSCs and LSECs to explore the molecular mechanisms that promote liver fibrosis. Our findings indicated that activated LX-2 cells release inflammatory factors which may be an important factor leading to the injury of LSECs.We found that activation of the cGAS-STING signaling pathway in HSCs triggers the release of pro-inflammatory factors, and aggravates the injury of LSECs, which promotes the formation of hepatic sinusoidal microthrombosis. Microthrombosis formation is a process involving multiple factors, which is closely associated with vascular endothelial integrity and function [27,28]. Our research demonstrated that the activation of the cGAS-STING signaling pathway aggravated the secretion of prothrombotic substances by LSECs. Based on our research results, inflammation and hepatic sinusoidal microthrombosis are tightly interrelated and LSEC-secreted prothrombotic substances accelerate the process. Due to the aggregation of red blood cells and platelets in hepatic sinuses, hepatic sinuses microthrombosis are formation, which further aggravates hepatic microcirculation disorder and promotes portal hypertention.

There is evidence that hepatic sinusoidal microthrombosis contributes to intrahepatic vascular resistance and promotes portal venous pressure [33,34]. Portal hypertension is determined by static structural remodeling (fibrosis and scarring) and dynamic intrahepatic resistance (contractile HSCs and endothelial dysfunction) [35,36]. However, limited information is available regarding the molecular drivers of PHT. In this study, we investigated potential modulators of hepatic sinusoidal microthrombosis in PHT. Assessment of the hepatic venous pressure gradient (HVPG) indirectly reflects the degree of portal pressure, which limits its wide application in clinical practice [37,38]. Here, we used the newest EUS-PPG method, which can directly measure portal vein and hepatic vein pressure; it can also evaluate pre-hepatic and pre-sinusoidal portal hypertension [39–41]. Previous research has found that EUS-PPG measurements provide excellent correlation with HVPG, histological hepatic fibrosis stage, and clinical markers of PTH [40–42]. The EUS-guided liver biopsy also can be performed safely during the same session as EUS-PPG, providing a comprehensive endoscopic evaluation of the patient with liver cirrhosis and portal hypertension [43]. A remarkable finding of the current study was that a linear relationship was observed between these prothrombotic substances and PPG. This direct relationship firstly suggests that hepatic sinusoidal microthrombosis has a pathogenic role in PHT. Expression of CXCL-1 in LSECs recruits neutrophils and promotes sinusoidal microthombosis, which increases portal venous pressure [34]. Previous studies found that reduced fibrin deposition and hepatic sinusoidal microthrombosis in the liver were observed in enoxaparin-treated cirrhotic rats [44]. Hepatic inflammation has effects on the sinusoidal network and can modulate intrahepatic vascular resistance [45–47]. Based on the above findings, we suspect that hepatic sinusoidal microthrombosis and inflammation may be involved in the development of portal hypertension.

In summary, our research indicates that activation of the cGAS-STING signaling pathway exacerbates intrahepatic inflammatory response and promotes liver fibrosis. It also leads to LSEC damage and expedites the formation of hepatic sinusoidal microthrombosis, which is a dynamic regulator of PPG in patients with liver fibrosis and PHT. These results suggest that the cGAS-STING signaling pathway may act as a potential therapeutic target for liver fibrosis.

CRediT authorship contribution statement

Shaobin Luo: Conceptualization, Data curation, Writing – original draft, Writing – review & editing, Supervision, Project administration. **Rongkun Luo:** Data curation, Formal analysis, Investigation, Methodology. **Huanyuan Lu:** Data curation, Formal analysis, Investigation, Methodology. **Rui Zhang:** Data curation, Formal analysis, Investigation,

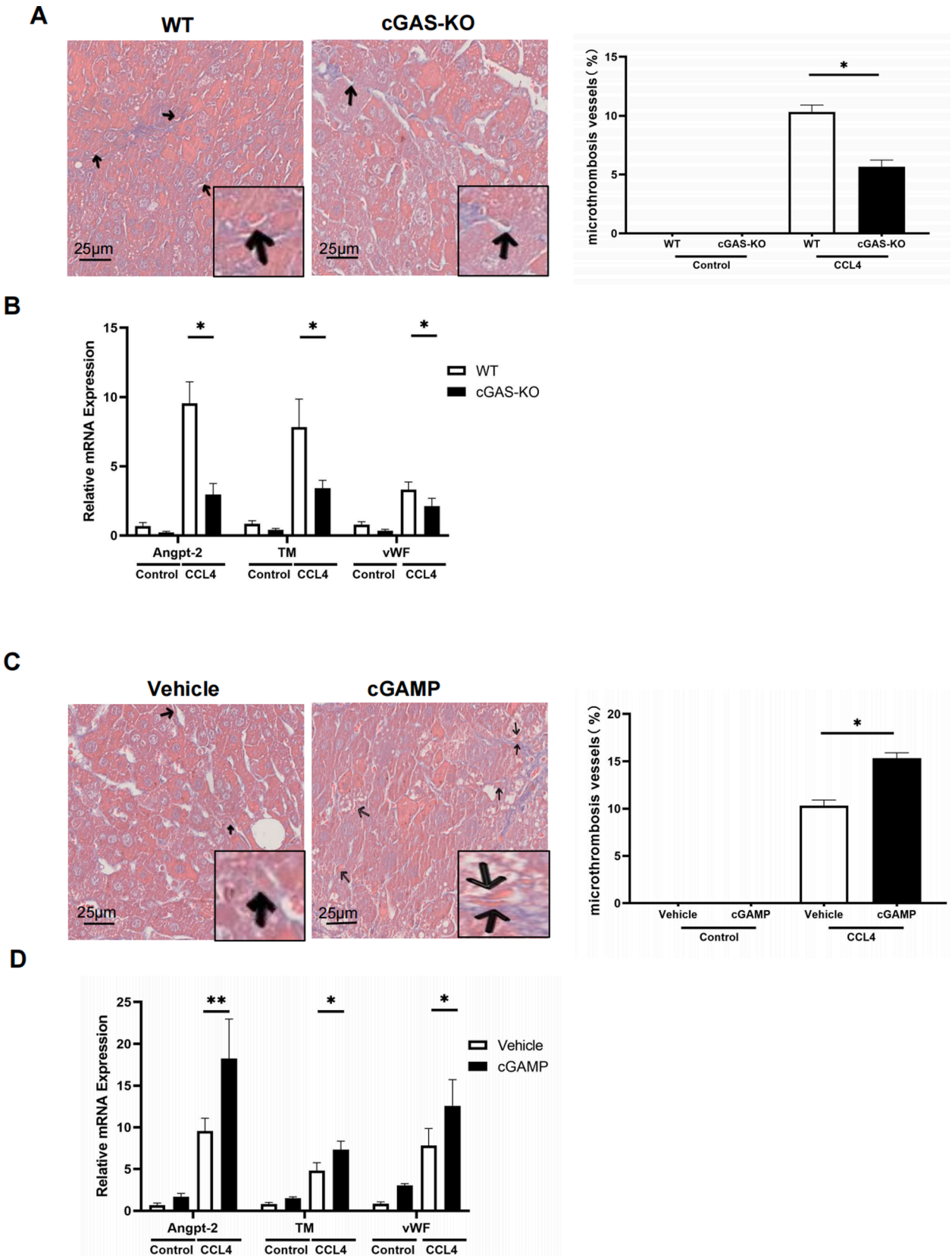

Fig. 9. cGAS-STING **signaling pathway promotes the formation of hepatic sinusoidal microthrombosis in fibrotic liver.** Masson's trichrome staining was used to evaluate hepatic sinusoidal microthrombosis in liver specimens from cGAS-KO and STING-activated mice administered CCl_4 for 8 weeks; the rate of positive vessel staining was measured (A and C). mRNA expression levels of Angpt-2, vWF, and TM were measured via RT-qPCR (B and D). *: $P < 0.05$; **: $P < 0.01$; ***: $P < 0.001$ vs. WT mice administered CCl_4.

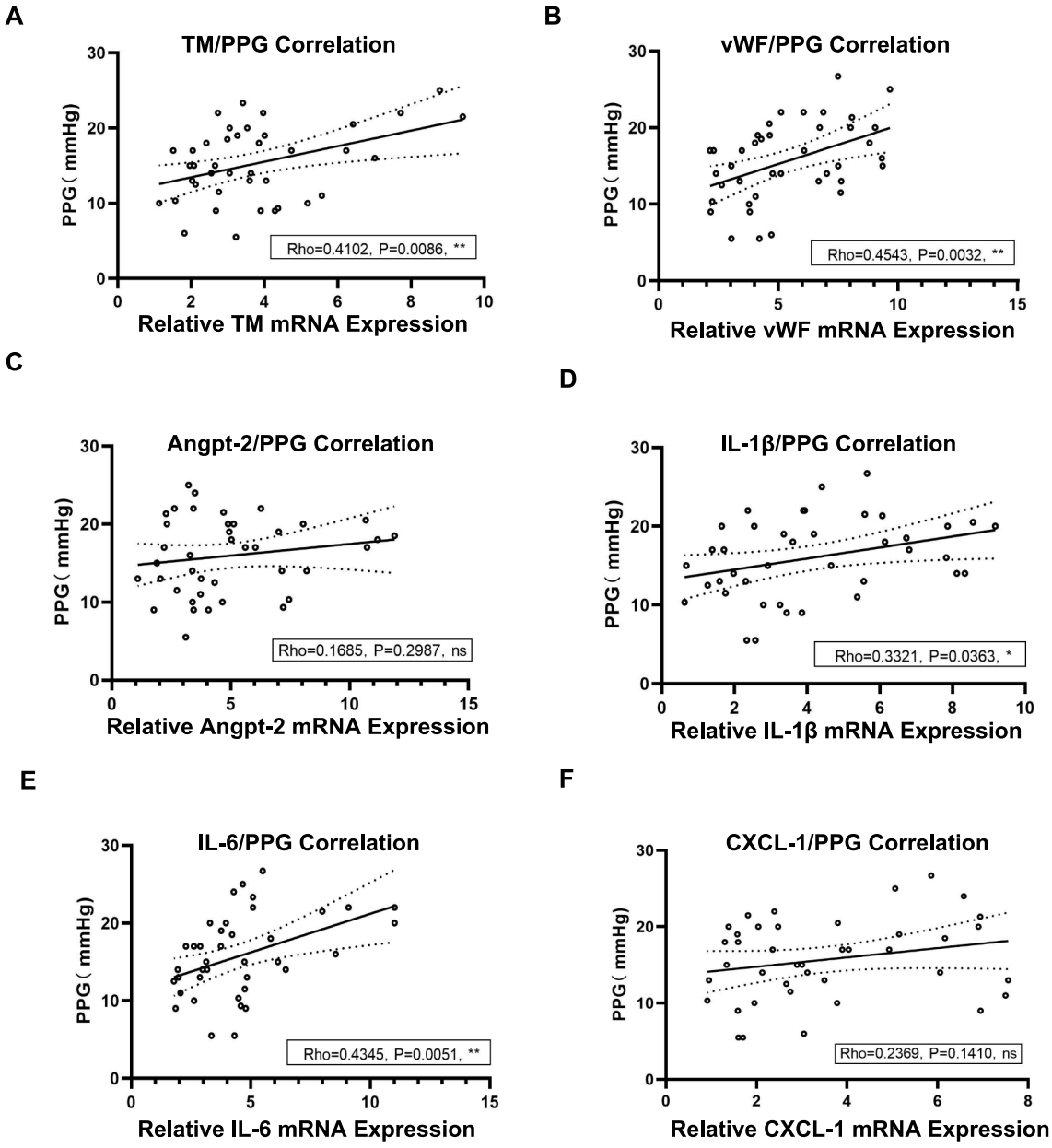

Fig. 10. Prothrombotic mediators are associated with EUS-PPG in human with liver fibrosis and PHT. PPG was measured by endoscopic ultrasound-guided portal vein puncture in patients with liver cirrhosis and PHT. Portal venous pressure gradient (PPG) versus serum mRNA levels of prothrombotic mediators (TM,vWF, Angpt-2) and inflammatory factors (IL-1β, IL-6, CXCL-1) (A–F). *: $P < 0.05$; **: $P < 0.01$; ***: $P < 0.001$.

Methodology. **Gang Deng:** Formal analysis, Writing – original draft, Writing – review & editing. **Hongwu Luo:** Formal analysis, Writing – original draft, Writing – review & editing. **Xiao Yu:** Formal analysis, Writing – original draft, Writing – review & editing. **Changfa Wang:** Validation, Software, Visualization. **Hui Zhang:** Validation, Software, Visualization. **Yuping Zhang:** Validation, Software, Visualization. **Wei Huang:** Validation, Software. **Jichun Sun:** Validation, Software. **Yinghong Liu:** Validation, Software. **Feizhou Huang:** Formal analysis, Methodology, Supervision. **Zhao Lei:** Conceptualization, Funding acquisition.

Declaration of competing interest

The authors declare that they have no known competing financial interests or personal relationships that could have appeared to influence the work reported in this paper.

Data availability

The authors are unable or have chosen not to specify which data has been used.

Appendix A. Supplementary material

Supplementary data to this article can be found online at https://doi.org/10.1016/j.intimp.2023.111132.

References

[1] R. Bataller, D.A. Brenner, Liver fibrosis, J. Clin. Invest. 115 (2005) 209–218.
[2] P. Angeli, A step forward in the choice of fluid for early resuscitation of critically ill patients with cirrhosis, Hep. Intl. 15 (2021) 858–859.
[3] V. Hernandez-Gea, S.L. Friedman, Pathogenesis of liver fibrosis, Annu. Rev. Pathol. 6 (2011) 425–456.

[4] Y. Koyama, D.A. Brenner, Liver inflammation and fibrosis, J. Clin. Invest. 127 (2017) 55–64.
[5] M. Ruart, L. Chavarria, G. Campreciós, N. Suárez-Herrera, C. Montironi, S. Guixé-Muntet, J. Bosch, et al., Impaired endothelial autophagy promotes liver fibrosis by aggravating the oxidative stress response during acute liver injury, J. Hepatol. 70 (2019) 458–469.
[6] M.K. Terkelsen, S.M. Bendixen, D. Hansen, E.A.H. Scott, A.F. Moeller, R. Nielsen, S. Mandrup, et al., Transcriptional dynamics of hepatic sinusoid-associated cells after liver injury, Hepatology 72 (2020) 2119–2133.
[7] J. Lv, C. Xing, Y. Chen, H. Bian, N. Lv, Z. Wang, M. Liu, et al., The STING in non-alcoholic fatty liver diseases: potential therapeutic targets in inflammation-carcinogenesis pathway, Pharmaceuticals (Basel) (2022) 15.
[8] L. Sun, J. Wu, F. Du, X. Chen, Z.J. Chen, Cyclic GMP-AMP synthase is a cytosolic DNA sensor that activates the type I interferon pathway, Science 339 (2013) 786–791.
[9] A. Ablasser, Z.J. Chen, cGAS in action: Expanding roles in immunity and inflammation, Science 363 (2019).
[10] X. Zhang, H. Shi, J. Wu, X. Zhang, L. Sun, C. Chen, Z.J. Chen, Cyclic GMP-AMP containing mixed phosphodiester linkages is an endogenous high-affinity ligand for STING, Mol. Cell 51 (2013) 226–235.
[11] J. Wu, L. Sun, X. Chen, F. Du, H. Shi, C. Chen, Z.J. Chen, Cyclic GMP-AMP is an endogenous second messenger in innate immune signaling by cytosolic DNA, Science 339 (2013) 826–830.
[12] B. Chen, X. Rao, X. Wang, Z. Luo, J. Wang, S. Sheng, Y. Liu, et al., cGAS-STING signaling pathway and liver disease: from basic research to clinical practice, Front. Pharmacol. 12 (2021), 719644.
[13] R. Chen, J. Du, H. Zhu, Q. Ling, The role of cGAS-STING signalling in liver diseases, JHEP Rep. 3 (2021), 100324.
[14] C.X. Sha, L.L. Ju, P. Zhou, D.F. Yao, M. Yao, Activation of cGAS/STING signaling pathway and its immunological role in the progression of nonalcoholic fatty liver disease, Zhonghua Gan Zang Bing Za Zhi 30 (2022) 564–568.
[15] Z. Wang, N. Chen, Z. Li, G. Xu, X. Zhan, J. Tang, X. Xiao, et al., The cytosolic DNA-sensing cGAS-STING pathway in liver diseases, Front. Cell Dev. Biol. 9 (2021), 717610.
[16] D. Xu, Y. Tian, Q. Xia, B. Ke, The cGAS-STING pathway: novel perspectives in liver diseases, Front. Immunol. 12 (2021), 682736.
[17] K. Ishak, A. Baptista, L. Bianchi, F. Callea, J. De Groote, F. Gudat, H. Denk, et al., Histological grading and staging of chronic hepatitis, J. Hepatol. 22 (1995) 696–699.
[18] J.Y. Huang, J.B. Samarasena, T. Tsujino, J. Lee, K.Q. Hu, C.E. McLaren, W.P. Chen, et al., EUS-guided portal pressure gradient measurement with a simple novel device: a human pilot study, Gastrointest. Endosc. 85 (2017) 996–1001.
[19] S.J. Higgins, K. De Ceunynck, J.A. Kellum, X. Chen, X. Gu, S.A. Chaudhry, S. Schulman, et al., Tie2 protects the vasculature against thrombus formation in systemic inflammation, J. Clin. Invest. 128 (2018) 1471–1484.
[20] E.M. Conway, Thrombomodulin and its role in inflammation, Semin. Immunopathol. 34 (2012) 107–125.
[21] J. Chen, D.W. Chung, Inflammation, von Willebrand factor, and ADAMTS13, Blood 132 (2018) 141–147.
[22] C. Comerford, S. Glavey, J. Quinn, J.M. O'Sullivan, The role of VWF/FVIII in thrombosis and cancer progression in multiple myeloma and other hematological malignancies, J. Thromb. Haemost. 20 (2022) 1766–1777.
[23] K. Katsumata, J. Ishihara, A. Mansurov, A. Ishihara, M.M. Raczy, E. Yuba, J. A. Hubbell, Targeting inflammatory sites through collagen affinity enhances the therapeutic efficacy of anti-inflammatory antibodies, Sci. Adv. (2019), 5:eaay1971.
[24] T. Tsuchida, S.L. Friedman, Mechanisms of hepatic stellate cell activation, Nat. Rev. Gastroenterol. Hepatol. 14 (2017) 397–411.
[25] Z. Lei, M. Deng, Z. Yi, Q. Sun, R.A. Shapiro, H. Xu, T. Li, et al., cGAS-mediated autophagy protects the liver from ischemia-reperfusion injury independently of STING, Am. J. Physiol. Gastrointest. Liver Physiol. 314 (2018) G655–G667.
[26] R. Shen, K. Yang, X. Cheng, C. Guo, X. Xing, H. Sun, D. Liu, et al., Accumulation of polystyrene microplastics induces liver fibrosis by activating cGAS/STING pathway, Environ. Pollut. 300 (2022), 118986.
[27] B. Han, X. Wang, P. Wu, H. Jiang, Q. Yang, S. Li, J. Li, et al., Pulmonary inflammatory and fibrogenic response induced by graphitized multi-walled carbon nanotube involved in cGAS-STING signaling pathway, J. Hazard. Mater. 417 (2021), 125984.
[28] J. Bai, F. Liu, cGAS–STING signaling and function in metabolism and kidney diseases, J. Mol. Cell Biol. 13 (2021) 728–738.
[29] C.Y. Lin, P. Adhikary, K. Cheng, Cellular protein markers, therapeutics, and drug delivery strategies in the treatment of diabetes-associated liver fibrosis, Adv. Drug Deliv. Rev. 174 (2021) 127–139.
[30] T.E. Fisher, T.A. Molskness, A. Villeda, M.B. Zelinski, R.L. Stouffer, J. Xu, Vascular endothelial growth factor and angiopoietin production by primate follicles during culture is a function of growth rate, gonadotrophin exposure and oxygen milieu, Hum. Reprod. 28 (2013) 3263–3270.
[31] E. Kostallari, V.H. Shah, Angiocrine signaling in the hepatic sinusoids in health and disease, Am. J. Physiol. Gastrointest. Liver Physiol. 311 (2016) G246–G251.
[32] Y. Iwakiri, J. Trebicka, Portal hypertension in cirrhosis: Pathophysiological mechanisms and therapy, JHEP Rep 3 (2021), 100316.
[33] E. Pandey, A.S. Nour, E.N. Harris, Prominent receptors of liver sinusoidal endothelial cells in liver homeostasis and disease, Front. Physiol. 11 (2020) 873.
[34] M.B. Hilscher, T. Sehrawat, J.P. Arab, Z. Zeng, J. Gao, M. Liu, E. Kostallari, et al., Mechanical stretch increases expression of CXCL1 in liver sinusoidal endothelial cells to recruit neutrophils, generate sinusoidal microthombi, and promote portal hypertension, Gastroenterology 157 (2019) 193–209.e199.
[35] M. Fernandez, M. Mejias, E. Garcia-Pras, R. Mendez, J.C. Garcia-Pagan, J. Bosch, Reversal of portal hypertension and hyperdynamic splanchnic circulation by combined vascular endothelial growth factor and platelet-derived growth factor blockade in rats, Hepatology 46 (2007) 1208–1217.
[36] L. Turco, G. Garcia-Tsao, Portal hypertension: pathogenesis and diagnosis, Clin. Liver Dis. 23 (2019) 573–587.
[37] J. Bosch, P. Pizcueta, F. Feu, M. Fernández, J.C. García-Pagán, Pathophysiology of portal hypertension, Gastroenterol. Clin. North Am. 21 (1992) 1–14.
[38] R. Khanna, S.K. Sarin, Non-cirrhotic portal hypertension - diagnosis and management, J. Hepatol. 60 (2014) 421–441.
[39] A.Y. Choi, K.J. Chang, J.B. Samarasena, J.G. Lee, X. Li, W. Guo, V.S. Chandan, et al., Endoscopic ultrasound-guided porto-systemic pressure gradient measurement correlates with histological hepatic fibrosis, Dig. Dis. Sci. (2022).
[40] W. Zhang, C. Peng, S. Zhang, S. Huang, S. Shen, G. Xu, F. Zhang, et al., EUS-guided portal pressure gradient measurement in patients with acute or subacute portal hypertension, Gastrointest. Endosc. 93 (2021) 565–572.
[41] J.Y. Huang, J.B. Samarasena, T. Tsujino, K.J. Chang, EUS-guided portal pressure gradient measurement with a novel 25-gauge needle device versus standard transjugular approach: a comparison animal study, Gastrointest. Endosc. 84 (2016) 358–362.
[42] A.Y. Choi, K.J. Chang, J.B. Samarasena, J.G. Lee, X. Li, W. Guo, V.S. Chandan, et al., Endoscopic ultrasound-guided porto-systemic pressure gradient measurement correlates with histological hepatic fibrosis, Dig. Dis. Sci. 67 (2022) 5685–5692.
[43] A.Y. Choi, J. Kolb, S. Shah, A. Chahine, R. Hashimoto, A. Patel, T. Tsujino, et al., Endoscopic ultrasound-guided portal pressure gradient with liver biopsy: 6 years of endo-hepatology in practice, J. Gastroenterol. Hepatol. 37 (2022) 1373–1379.
[44] F. Cerini, M. Vilaseca, E. Lafoz, O. García-Irigoyen, H. García-Calderó, D. M. Tripathi, M. Avila, et al., Enoxaparin reduces hepatic vascular resistance and portal pressure in cirrhotic rats, J. Hepatol. 64 (2016) 834–842.
[45] C. Engelmann, J. Clària, G. Szabo, J. Bosch, M. Bernardi, Pathophysiology of decompensated cirrhosis: Portal hypertension, circulatory dysfunction, inflammation, metabolism and mitochondrial dysfunction, J. Hepatol. 75 (Suppl 1) (2021) S49–S66.
[46] G. Mehta, T. Gustot, R.P. Mookerjee, J.C. Garcia-Pagan, M.B. Fallon, V.H. Shah, R. Moreau, et al., Inflammation and portal hypertension - the undiscovered country, J. Hepatol. 61 (2014) 155–163.
[47] A. Lemmers, T. Gustot, A. Durnez, S. Evrard, C. Moreno, E. Quertinmont, V. Vercruysse, et al., An inhibitor of interleukin-6 trans-signalling, sgp130, contributes to impaired acute phase response in human chronic liver disease, Clin. Exp. Immunol. 156 (2009) 518–527.